

Measurement of non-monotonous phase changes in temporal speckle pattern interferometry using a correlation method without a temporal carrier

Lucas P. Tendela^{a,*}, Gustavo E. Galizzi^a, Alejandro Federico^b, Guillermo H. Kaufmann^{a,c}

^a Instituto de Física Rosario, Blvd. 27 de Febrero 210 bis, S2000EZF Rosario, Argentina

^b Electrónica e Informática, Instituto Nacional de Tecnología Industrial, P.O. Box B1650WAB, B1650KNA San Martín, Argentina

^c Centro Internacional Franco Argentino de Ciencias de la Información y de Sistemas, Blvd. 27 de Febrero 210 bis, S2000EZF Rosario, Argentina

ARTICLE INFO

Article history:

Received 12 December 2014

Received in revised form

25 March 2015

Accepted 26 March 2015

Available online 20 April 2015

Keywords:

Temporal speckle pattern interferometry

Phase evaluation

Order statistics correlation coefficient

Non-monotonous phase changes

ABSTRACT

Recently, a phase evaluation method was proposed to measure nanometric displacements by means of digital speckle pattern interferometry when the phase change introduced by the deformation is in the range $[0, \pi]$ rad. This method is based on the evaluation of a correlation coefficient between two speckle interferograms generated by both deformation states of the object. In this paper, we present a novel technique to measure non-monotonous displacements in temporal speckle pattern interferometry using a correlation method without a temporal carrier. In this approach, the sign ambiguity is resolved automatically due to the introduction of a function that determines the correct sign of the displacement between two consecutive speckle interferograms. The rms phase errors introduced by the proposed method are determined using computer-simulated speckle interferograms. An application of the phase retrieval method to process experimental data is also presented.

© 2015 Elsevier Ltd. All rights reserved.

1. Introduction

Temporal speckle pattern interferometry (TSPI) is a non-contact technique for measuring static and dynamic deformation fields from the processing of the optical phase information generated by diffusely reflecting objects [1]. Its main advantages include its high sensitivity, and the possibility of real time and whole-field measurement [2]. In this technique, a sequence of speckle interferograms is recorded throughout the entire deformation history of the object under study, and the optical phase distribution is coded in the temporal intensity modulation, which is recorded by means of a CCD detector [1].

Until recently, the most common phase recovery techniques used in TSPI were temporal phase-shifting and Fourier transform methods [3–5]. When the phase changes are non-monotonous these methods also need the introduction of temporal carrier fringes to overcome the sign ambiguity [1]. While there exist various ways of introducing temporal carrier fringes in the optical setup, most procedures complicate the automation of the interferometer operation [6,7].

On the other hand, the rapid miniaturization of micro-electro-mechanical systems (MEMS), micro-sensors and micro-optical devices has raised new challenges in the development of non-destructive and non-contact testing methods [8], not only in the development phase but also during the entire manufacturing process, even when they are under service. Therefore, full-field and non-invasive methods are desirable to study material properties and parameters [9,10].

It should be noted that in many cases when MEMS are analyzed, the wrapped phase map does not present the usual 2π phase discontinuities [11], i.e., the generated correlation fringes show less than one fringe. Therefore, it is not necessary to apply a spatial phase unwrapping algorithm to obtain the continuous phase distribution. Recently, in Ref. [12] was proposed a novel phase evaluation method to measure nanometric displacements by means of DSPI when the phase change introduced by the specimen deformation is in the range $[0, \pi]$ rad. This last phase retrieval technique is based on the calculation of a correlation coefficient between the two speckle interferograms generated by both deformation states of the object. Although the approach presented in Ref. [12] does not need the introduction of a phase-shifting facility or spatial carrier fringes in the optical setup, the intensities of the object and the reference beams corresponding to both the initial and the deformed interferograms must be recorded. It should also be noted that this limitation complicates the automatic operation of the interferometer. Moreover, this limitation does not allow the application of this method for the analysis of non-repeatable

* Corresponding author. Tel.: +54 341 485 3200x455; fax: +54 341 480 8584.

E-mail address: tendela@ifir-conicet.gov.ar (L.P. Tendela).

dynamic events by recording a sequence of interferograms throughout the entire deformation history of the testing object.

More recently, Tendela et al. [13] have presented a phase retrieval method based on the approach reported in Ref. [12] to be used in a DSPI. In this method there is no need to record the intensities of the object and the reference beams corresponding to both the initial and the deformed interferograms. However, when the technique proposed in Ref. [13] is used to measure non-monotonous phase changes by means of TSPI, this method also needs the introduction of temporal carrier fringes to overcome the sign ambiguity.

In this paper we propose a phase retrieval approach to be used in a TSPI system based on the correlation method reported in Ref. [13]. The main highlight of this novel approach is that the sign ambiguity is resolved automatically due to the introduction of a function that determines the correct sign of the displacement between two consecutive speckle interferograms. Therefore, when this approach is applied, the introduction of temporal carrier fringes to overcome the sign ambiguity is not needed, thus allowing its application for the analysis of non-repeatable dynamic events.

In the following section, a description of the proposed method is presented. Afterwards, its performance is analyzed by means of computer-simulated speckle interferograms for the case of out-of-plane displacements, using the similar approach applied in Ref. [12]. This analysis allows us to evaluate the rms phase errors introduced by the proposed method. Finally, an application of the phase retrieval technique to process experimental data is also illustrated by analyzing the out-of-plane displacement field generated by the movement of a metal plate.

2. Theoretical concepts

In a TSPI system, the intensity distribution $I(x, y, t)$ at a pixel (x, y) and frame t recorded by the CCD camera is given by

$$I(x, y, t) = I_0(x, y, t) + I_M(x, y, t) \cos[\phi_s(x, y) + \Delta\phi(x, y, t)], \quad (1)$$

where $I_0(x, y, t)$ is the intensity bias, $I_M(x, y, t)$ is the modulation intensity, $x = 1, 2, \dots, n_x$ and $y = 1, 2, \dots, n_y$ are the spatial coordinates of the camera pixels, $t = 1, 2, \dots, n_t$ is the temporal coordinate, $\phi_s(x, y)$ accounts for the random change in the optical path due to the roughness of the scattering surface, and $\Delta\phi(x, y, t)$ corresponds to the deterministic change in the path to be measured, introduced by the underwent deformation.

When the phase change $\Delta\phi$ produced by the deformation between two successive frames corresponding to the times $t = t_m$ and $t = t_{m+1}$, where $t_m = 1, 2, \dots, n_t - 1$, is lower than π , it can be estimated as [13]

$$\Delta\phi(x, y, t_m, t_{m+1}) = a \cos[C_{OS}[I(x, y, t_m), I(x, y, t_{m+1})]], \quad (2)$$

where C_{OS} is the order statistics correlation coefficient defined in Ref. [14].

If the phase changes are monotonous, the total phase change $\Delta\Phi(x, y)$ can be determined as

$$\Delta\Phi(x, y) = \sum_{i=1}^{n_t-1} \Delta\phi(x, y, t_i, t_{i+1}). \quad (3)$$

However, when the phase changes are non-monotonous, the total phase $\Delta\Phi(x, y)$ cannot be computed using Eq. (3) due to the undetermined sign of $\Delta\phi(x, y, t_i, t_{i+1})$.

In order to overcome the above mentioned limitation for retrieving the phase change, it is proposed the evaluation of an estimator $\tilde{\Delta\phi}$ which is based on the introduction of a modulation intensity $I_0^*(x, y)$ in Eq. (2), and a function $S(x, y, t_m, t_{m+1})$ in Eq. (3). The modulation intensity is obtained by recording separately the intensities of the object and the reference beams corresponding at any time of the experiment, i.e. it is considered constant for all

frames. Its main function is to reduce the rms phase error σ when the number of frames increases. The function S is added to Eq. (3) to determine the sign of the displacement. The validity of the proposed phase retrieval method will be demonstrated in Sections 4 and 5 by using numerical simulations and also experimental data, respectively.

Therefore, the estimated phase change $\tilde{\Delta\phi}$ introduced by the deformation between two successive frames, $I(t_m)$ and $I(t_{m+1})$, can be evaluated as

$$\tilde{\Delta\phi}(t_m, t_{m+1}) = a \cos[C_{OS}[I(t_m) - I_0^*, I(t_{m+1}) - I_0^*]], \quad (4)$$

where the spatial coordinates along the horizontal and vertical directions were omitted for the sake of clarity.

To compute the estimated phase change between both recorded interferograms by means of Eq. (4), the calculation was performed pixel by pixel. This process consisted simply of moving a sliding window of size $L \times L$ from point to point in the horizontal and vertical directions. For each pixel, two new subimages $I_L(t_m)$ and $I_L(t_{m+1})$ of size $L \times L$ are obtained from $I(t_m)$ and $I(t_{m+1})$, respectively.

Finally, the estimated total phase change can be computed as

$$\tilde{\Delta\Phi} = \sum_{i=1}^{n_t-1} S(t_i, t_{i+1}) \tilde{\Delta\phi}(t_i, t_{i+1}), \quad (5)$$

where $S(t_m, t_{m+1})$ determines the sign of the estimated phase change $\Delta\phi$ between two successive frames, and its evaluation will be described in the following paragraphs.

Considering the first frame $t=1$, by using Eq. (1) the intensity distribution $I(1)$ is given by

$$I(1) = I_0(1) + I_M(1) \cos \phi_s. \quad (6)$$

In the second frame $t=2$, the underwent deformation has introduced a phase change $\Delta\phi(1, 2)$ between both frames. In this case, the intensity distribution $I(2)$ is written as

$$I(2) = I_0(2) + I_M(2) \cos[\phi_s + \Delta\phi(1, 2)], \quad (7)$$

where the phase change $\Delta\phi(1, 2)$ is computed by means of Eq. (4).

It should be noted that the random phase ϕ_s must be determined using a different technique, being the phase-shifting and the Fourier transform methods the most commonly used approaches [1]. In order to avoid the introduction of a phase-shifting facility in the optical setup, if a high speed camera is used and if the deformation experimented by the testing object does not vary rapidly with time, it is possible to assume that the phase changes between the first four successive frames are all equal, and the Carré phase-shifting technique can be applied to determine the random phase ϕ_s .

Also, assuming that the bias and the modulation intensities are the same between both frames, that is

$$I_0(1) = I_0(2) = I_0, \quad (8)$$

$$I_M(1) = I_M(2) = I_M, \quad (9)$$

using some trigonometric properties, Eqs. (6) and (7) can be expressed as a function of $\cos \Delta\phi(1, 2)$ and $\sin \Delta\phi(1, 2)$ as

$$I(1) = I_0 + I_M \cos \phi_s, \quad (10)$$

$$I(2) = I_0 + I_M \cos \phi_s \cos \Delta\phi(1, 2) - I_M \sin \phi_s \sin \Delta\phi(1, 2). \quad (11)$$

Substituting Eq. (10) into Eq. (11), after some mathematical manipulations the intensity distribution $I(2)$ can be written as

$$I(2) = I_0 + [I(1) - I_0] \cos \Delta\phi(1, 2) - I_M \sin \phi_s \sin \Delta\phi(1, 2). \quad (12)$$

As we want to know the sign of $\Delta\phi(1, 2)$, considering that the cosine function is even, it is only necessary to know the sign of

$\sin \Delta\phi(1, 2)$. Therefore, Eq. (12) can be expressed as

$$I_M \sin \phi_s \sin \Delta\phi(1, 2) = I_0 + [I(1) - I_0] \cos \Delta\phi(1, 2) - I(2). \quad (13)$$

Taking into account that the modulation intensity I_M is a positive magnitude, the sign of $\Delta\phi(1, 2)$ can be computed as

$$\begin{aligned} S(1, 2) &= \text{sign}(\sin \Delta\phi(1, 2)) \\ &= \text{sign}(\sin \phi_s) \times \text{sign}[I_0 + [I(1) - I_0] \cos \Delta\phi(1, 2) - I(2)], \end{aligned} \quad (14)$$

where sign is the sign function.

Therefore, the total phase between the first two frames $\Phi(1)$ can be written as

$$\Phi(1) = \phi_s + S(1, 2)\Delta\phi(1, 2). \quad (15)$$

For the third frame $t=3$, a new deformation has occurred, introducing a phase change $\Delta\phi(2, 3)$ between the frames $t=2$ and $t=3$. Considering that the bias and the modulation intensities are constant for all the frames, the intensity distribution $I(3)$ can be computed as

$$I(3) = I_0 + I_M \cos[\Phi(1) + \Delta\phi(2, 3)]. \quad (16)$$

As before, the phase change $\Delta\phi(2, 3)$ is computed by means of Eq. (4), and the intensity distribution $I(3)$ can be written as

$$I(3) = I_0 + [I(2) - I_0] \cos \Delta\phi(2, 3) - I_M \sin \Phi(1) \sin \Delta\phi(2, 3). \quad (17)$$

In this case, it is necessary to know the sign of $\sin \Delta\phi(2, 3)$. Therefore, Eq. (17) is expressed as

$$I_M \sin \Phi(1) \sin \Delta\phi(2, 3) = I_0 + [I(2) - I_0] \cos \Delta\phi(2, 3) - I(3), \quad (18)$$

and the sign of $\sin \Delta\phi(2, 3)$ can be computed as

$$\begin{aligned} S(2, 3) &= \text{sign}(\sin \Delta\phi(2, 3)) \\ &= \text{sign}(\sin \Phi(1)) \times \text{sign}[I_0 + [I(2) - I_0] \cos \Delta\phi(2, 3) - I(3)]. \end{aligned} \quad (19)$$

Finally, the total phase between the first three frames $\Phi(2)$ can be written as

$$\Phi(2) = \phi_s + S(1, 2)\Delta\phi(1, 2) + S(2, 3)\Delta\phi(2, 3). \quad (20)$$

Therefore, if the random phase ϕ_s is known and $\Delta\phi(t_m, t_{m+1})$ is computed by means of Eq. (4), the function $S(t_m, t_{m+1})$ between any pair of successive frames $t = t_m$ and $t = t_{m+1}$ is given by

$$\begin{aligned} S(t_m, t_{m+1}) &= \text{sign}(\sin \Phi(t_m)) \\ &\times \text{sign}[I_0 + [I(t_m) - I_0] \cos \Delta\phi(t_m, t_{m+1}) - I(t_{m+1})]. \end{aligned} \quad (21)$$

As mentioned before, the number of pixels along the horizontal and vertical directions was omitted for the sake of clarity. Also, it is important to note that this method does not generate phase values over the first and the last L pixels. The consequences of this limitation will be discussed in Sections 4 and 5.

3. Numerical simulations

To evaluate the performance of the proposed phase retrieval technique, computer-simulated speckle interferograms were generated using the similar approach applied in Ref. [12]. As described before, this approach allows us to know precisely the original phase distribution and therefore, to determine the errors introduced by the algorithm proposed to evaluate the phase change.

Considering the 4f optical configuration of an out-of-plane speckle interferometer, any given point in the detector plane receives contributions from all the scattering centers in the input plane, which are large enough so that the complex amplitude can be described by the usual Gaussian first-order speckle statistics. The first lens performs a Fourier transform to the aperture plane in which a circular aperture acting as a low pass filter represents the contribution of the lens pupil in the final intensity distribution. The second lens performs another Fourier transformation which gives the complex amplitude at the detector plane. With this model, the intensity $I(x, y, t)$ of each speckle

interferogram can be simulated as [15]

$$I(x, y, t) = \left| R \exp(j\alpha) + F^{-1} HF \{ \exp[j(\phi_s(x, y) + \Phi_o(x, y, t))] \} \right|^2, \quad (22)$$

where R and α are the amplitude and phase of the reference beam, respectively, j is the imaginary unit, ϕ_s is a random variable with uniform distribution in $(-\pi, \pi]$, F and F^{-1} denote the direct and inverse 2-D Fourier transform, respectively, and Φ_o is the original total phase distribution. H is a circular low pass filter defined as

$$H(\rho) = \begin{cases} 1 & \rho \leq D/2 \\ 0 & \rho > D/2, \end{cases} \quad (23)$$

where D is the pupil diameter and ρ is the modulus of the position vector in the pupil plane.

In all numerical tests, each speckle interferogram was simulated for a resolution of $n_x = n_y = 512$ pixels in a scale of 256 gray levels with an average speckle size of 1 pixel, and each data set contained 512 images.

As previously expressed, the simulation method allows us to know precisely the original phase distribution, so that the errors generated by the approximations described in the previous section can be evaluated. The total phase change $\Delta\Phi$ estimated with the proposed method was compared with the original total phase change $\Delta\Phi_o$, allowing us to evaluate the rms phase error σ from

$$\sigma = \left\{ \frac{1}{n_x n_y n_t} \sum_{n_t=1}^{n_t=512} \sum_{n_x=1}^{n_x=512} \sum_{n_y=1}^{n_y=512} [e(x, y, t) - \langle e \rangle]^2 \right\}^{1/2}, \quad (24)$$

where the error matrix $e(x, y, t)$ is defined by

$$e(x, y, t) = |\Delta\tilde{\Phi}(x, y, t) - \Delta\Phi_o(x, y, t)|, \quad (25)$$

and $\langle e \rangle$ the mean value of the matrix e .

Additionally, the performance of the proposed phase retrieval method was also compared with the one given by the Fourier transform technique [1].

4. Numerical results

The proposed phase retrieval method was tested using different simulated phase distributions. For the case of an out-of-plane linear increasing phase change of 0.83 rad per frame, Fig. 1 shows the plot of the temporal evolution of the retrieved phase distribution estimated with the proposed approach (bold curve) for the central pixel of the pattern. In this case, the correlation was evaluated using a sliding window of size 65×65 pixels. For comparison, the same figure also displays the original input phase map $\Delta\Phi_o$ (solid circles) and the phase distribution (dash-dot line) retrieved by means of Eq. (3).

In this example, the rms phase error obtained using the proposed approach given by Eq. (5) was $\sigma = 0.02$ rad and with Eq. (3) was $\sigma = 4.15$ rad. In this case, it can be noted that the modulation intensity I_0^* has to be taken into account when the phase change is computed. For comparison, the phase distribution was also computed using the well known Fourier Transform method (not shown in Fig. 1) and an rms phase error $\sigma = 0.22$ rad was obtained. Therefore, this example clearly shows that the proposed method outperforms the Fourier Transform technique.

As another typical example, Fig. 2 shows the plot of the retrieved phase distribution estimated with the proposed approach (bold curve) for the central pixel of the pattern, corresponding to a simulated non-monotonous out-of-plane parabolic displacement where the maximum phase change was approximately 60 rad. As before, the correlation was evaluated using a sliding window of size $L^2 = 65 \times 65$ pixels. For comparison, Fig. 2 also displays the original input phase map (solid circles) and the phase distribution obtained using the Fourier Transform method (dash line). It can be seen that

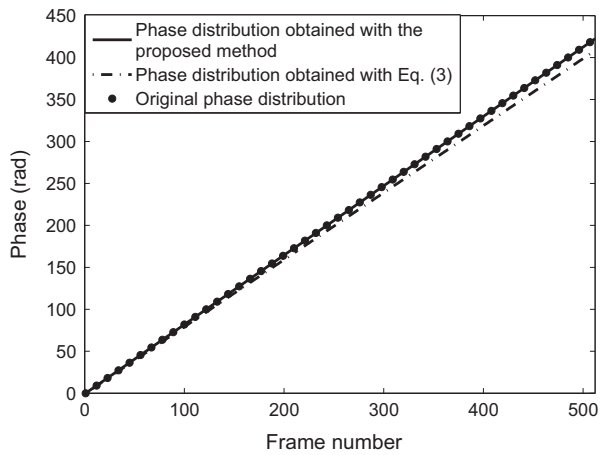


Fig. 1. Comparison between the temporal evolution of the original phase change $\Delta\phi_0$ (solid circles), the retrieved phase distribution (dash-dot line) obtained with Eq. (3) and the one estimated with the proposed method (bold curve) for the central pixel of the pattern, using a sliding window of size 65×65 pixels, corresponding to a simulated out-of-plane with a linear increasing phase change of 0.83 rad per frame.

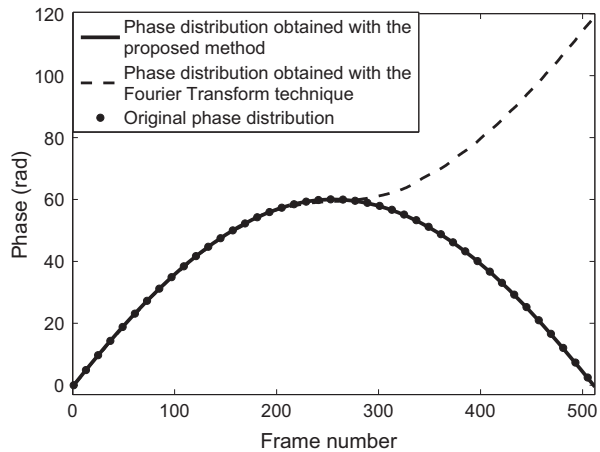


Fig. 2. Comparison between the temporal evolution of the original phase change $\Delta\phi_0$ (solid circles), the phase distribution obtained using the Fourier transform technique (dash line) and the retrieved phase distribution estimated with the proposed method (bold curve) for the central pixel of the pattern, using a sliding window of size 65×65 pixels and corresponding to a simulated out-of-plane parabolic displacement where the maximum phase change is approximately 60 rad.

this last method does not recover the phase change correctly. In this second example, the rms phase error obtained using the proposed technique was $\sigma = 0.06$ rad.

Furthermore, Fig. 3 shows the phase recovered with the proposed technique for pixels in the central column of the image. It should be noticed that the proposed technique recovers the displacement with its correct sign.

As mentioned in Section 2, Fig. 3 shows that the proposed method does not generate phase values over the first and last L pixels. This is a similar limitation given by the techniques reported in Refs. [12,13], which do not compute phase values over the first and last $L/2$ pixels. As it was mentioned in these papers, it is not a trivial issue to ascertain the window size that must be used as it depends on the shape of the phase distribution to be evaluated. In general, larger sliding windows are usually preferred to smooth the retrieved phase map to be obtained. However, larger windows also tend to reduce small bumps that may appear in the phase map. It must be taken into account that as the sliding window is displaced pixel by pixel in the horizontal and vertical directions,

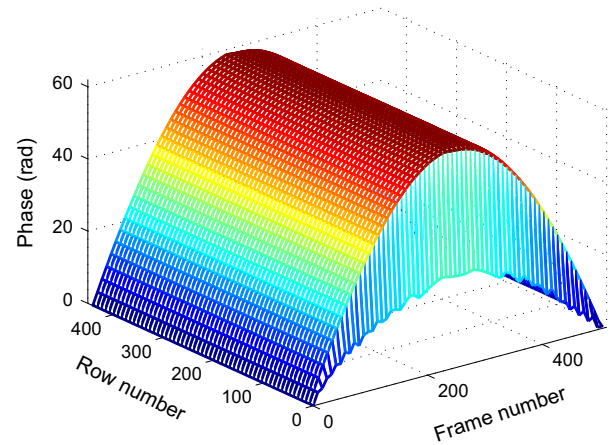


Fig. 3. Temporal evolution of the phase distribution evaluated using the proposed approach for pixels in the central column of the image, corresponding to the same simulation shown in Fig. 2.

Table 1

Rms phase error σ using different maximum phase values and window sizes obtained with the proposed method.

Maximum phase values (rad)	Window side (pixels)		
	16 × 16	32 × 32	64 × 64
	σ (rad)	σ (rad)	σ (rad)
12.01	0.73	0.32	0.30
36.03	0.23	0.05	0.05
60.05	0.35	0.07	0.06
90.08	1.73	0.15	0.07
108.09	8.25	2.75	1.05

the loss of information that is produced is negligible but the improvement in the signal-to-noise ratio is quite high.

Finally, to analyze the performance of the proposed phase retrieval technique, several non-monotonous out-of-plane parabolic displacement fields were simulated corresponding to different maximum phase values. Some of the results obtained from this numerical analysis corresponding to different window sizes are summarized in Table 1. It must be mentioned that a first sliding window was used to compute the estimated phase change $\Delta\phi$, and a second window was used to determine its sign, therefore, the rms phase error was computed without taking into account the first and last L rows and columns of each speckle interferogram. Looking at the numerical results listed in this table, it should be noted that the rms phase error strongly depends on the window size used to retrieve the phase distribution, that is the rms phase error decreases when the size of the sliding window increases. It is also seen that although the rms phase errors generated by the three phase retrieval approaches are quite low, they increase with the deformation amplitude.

5. Experimental results

To illustrate the performance of the phase retrieval approach when experimental data are processed, a TSPI system was used to measure the out-of-plane displacement component w generated by an aluminium plate attached to a piezoelectric transducer (PZT), which was programmed to displace linearly moving closer and farther from the CCD camera. Fig. 4 shows a schematic view of the TSPI system, which was based on a conventional out-of-plane speckle

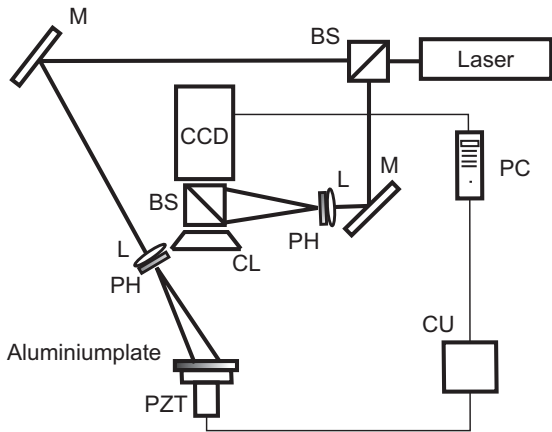


Fig. 4. Optical arrangement of the out-of-plane temporal speckle pattern interferometer: mirrors (M), piezoelectric transducer (PZT), microscope objectives (L), beam splitters (BS), pin holes (PH), camera lens (CL), control unit (CU), personal computer (PC).

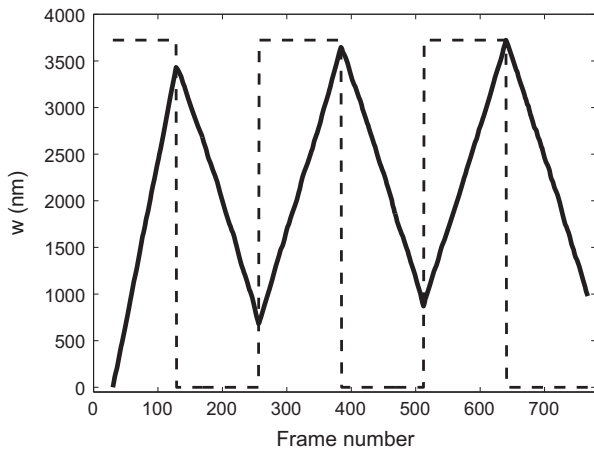


Fig. 5. Temporal evolution of the obtained displacement field for the central pixel of the image (bold line) using a sliding window of size 65×65 pixels, when the aluminium plate was linearly moving closer and farther from the CCD camera with steps of approximately 35 nm per frame. The same figure also shows the voltage difference applied between the successive frames to the PZT (in dash line and without units).

interferometer illuminated by a Nd:YAG laser with a wavelength $\lambda = 532.8$ nm, whose output was divided into the object and reference beams by a beam-splitter (BS). The reference beam was expanded by a microscope objective (L) and directed through another beam-splitter into the CCD camera (PulnixTM-765), where it was recombined with the light scattered by the object surface. In order to obtain a uniform illumination intensity, a pin hole (PH) was used in both object and reference beams. The angle between the direction of illumination and the normal to the surface of the object was $\gamma = 10^\circ$. A control unit (CU) applies a voltage to the PZT using an open loop control scheme. The applied voltage generates a displacement of the specimen that is the same for every point of the object surface. The camera output was fed to a frame grabber located inside a personal computer (PC) that digitizes the images in grey levels with a resolution of 512×512 pixels \times 8 bits, and each data set contained 768 images. The image acquisition system and the CU, which generates the displacement of the PZT, are controlled by the personal computer. The video camera had a zoom lens which allows us to image a small region of the specimen of approximately 23×23 mm² in size and for an average speckle size of 1 pixel.

In order to determine the displacement field, the phase change $\Delta\tilde{\phi}(t_m, t_{m+1})$ produced by the deformation between the two successive frames corresponding to times $t = t_m$ and $t = t_{m+1}$

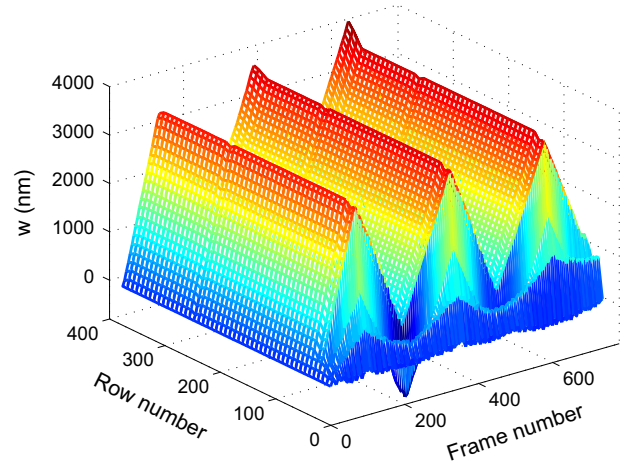


Fig. 6. Temporal evolution of the out-of-plane displacement field w evaluated using the proposed approach for pixels in the central column of the image, corresponding to the same measurement shown in Fig. 5.

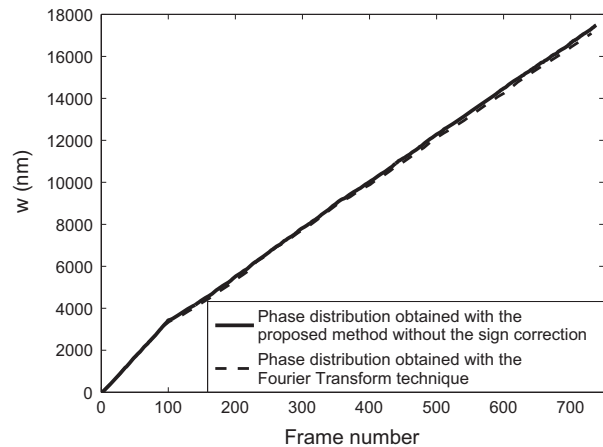


Fig. 7. Comparison between the temporal evolution of the displacement field obtained by means of the Fourier transform technique (dash line) and the one obtained by means of the proposed method (bold curve) without the sign correction, corresponding to the same measurement shown in Fig. 5.

was estimated using Eq. (4) and the out-of-plane displacement component $w(t_m, t_{m+1})$ was finally computed from [16]

$$w(t_m, t_{m+1}) = \frac{\lambda}{2\pi(1 + \cos \gamma)} \Delta\tilde{\phi}(t_m, t_{m+1}). \quad (26)$$

Fig. 5 depicts the temporal evolution of the obtained displacement field for the central pixel of the image (bold line). In this case, the correlation was evaluated using a sliding window of size 65×65 pixels and the displacement field was evaluated using the proposed method by means of Eq. (26). It must be noted that as the PZT used an open loop control scheme, we could not guarantee the precision of the displacement of the aluminium plate. The same figure also shows that the maximum value of the triangular curve of the displacement increases as the PZT runs, which could be related to a hysteresis cycle. To show that the phase distribution is recovered with its correct sign, Fig. 5 also depicts the voltage difference applied to the PZT between the successive frames (in dash line and without units). Therefore, the change in the slope of the displacement field corresponds to a change in the applied voltage difference, which means that the direction of the displacement had changed.

As mentioned in Section 2, in order to avoid the introduction of a phase-shifting facility in the optical setup, the random phase ϕ_s was

determined using the Carré phase-shifting considering that phase changes between the first four successive frames are all equal.

Fig. 6 shows the phase recovered with the proposed technique for the pixels in the central column of the image. It can be seen that the change of phase is approximately similar for every pixel in the column. As previously mentioned, the proposed method does not give phase values over the first and the last 65 pixels due to the size of the sliding window used to calculate the correlation and its sign. As described in Section 4, it should be noticed that this novel technique recovers the displacement with its correct sign.

In addition, to assess the accuracy of the proposed phase retrieval approach when experimental data was used, Fig. 7 shows the temporal evolution of the obtained displacement field for the central pixel of the image (bold line) without the sign correction, which is compared with the displacement field recovered with the Fourier transform technique (dash line). In this figure, it can be seen that the displacement field obtained with both techniques are quite similar.

6. Conclusions

In this paper we propose a novel phase evaluation method to be used in TSPI to measure non-monotonous displacements using a correlation method without introducing a temporal carrier. Using the proposed approach, the sign ambiguity is resolved automatically due to the introduction of a function that determines the correct sign of the displacement between two consecutive speckle interferograms. Therefore, this phase evaluation method does not need the introduction of a phase-shifting facility or temporal carrier fringes in the optical setup. This advantage not only makes easier the automation of the interferometer operation, but also allows the application of the proposed method to the analysis of non-repeatable dynamic events by recording a sequence of interferograms throughout the entire deformation history of the testing object.

The performance of the phase retrieval approach is investigated using different computer-simulated phase changes per frame and window sizes, approach which allows us to evaluate the rms phase errors. The numerical results presented in this work show that the performance of the proposed method outperforms the widely-known Fourier Transform technique. Finally, these results given by the numerical analysis are confirmed by processing experimental data obtained from the analysis of an aluminium plate when it is

attached to a piezoelectric transducer which was programmed to displace linearly moving closer and farther from the CCD camera.

References

- [1] Huntley JM. Automatic analysis of speckle interferograms. In: Rastogi PK, editor. *Digital speckle pattern interferometry and related techniques*. Chichester, New York: Wiley; 2001. p. 59–139.
- [2] Osten W, editor. *Optical inspection of microsystems*. Boca Raton: Taylor and Francis; 2007.
- [3] Kaufmann GH. Nondestructive testing with thermal waves using phase shifted temporal speckle pattern interferometry. *Opt Eng* 2003;42:2010–4.
- [4] Takeda M, Ina H, Kobayashi S. Fourier-transform method of fringe-pattern analysis for computer-based topography and interferometry. *J Opt Soc Am* 1982;72:156–60.
- [5] Kaufmann GH, Galizzi GE. Phase measurement in temporal speckle pattern interferometry: comparison between the phase-shifting and the Fourier transform methods. *Appl Opt* 2002;41:7254–63.
- [6] Kaufmann GH. Phase measurement in temporal speckle pattern interferometry using the Fourier transform method with and without a temporal carrier. *Opt Commun* 2003;217:141–9.
- [7] Dorrió BV, Fernández JL. Phase-evaluation methods in whole-field optical measurement techniques. *Meas Sci Technol* 1999;10:R35–55.
- [8] Höfling R, Aswendt P. Speckle metrology for microsystem inspection. In: Osten W, editor. *Optical inspection of microsystems*. Boca Raton: Taylor & Francis; 2007. p. 427–58.
- [9] Seebacher S, Osten W, Baumbach T, Jüptner W. The determination of material parameters of microcomponents using digital holography. *Opt Lasers Eng* 2001;36:103–26.
- [10] Hill M, O'Mahony C, Berney H, Hughes PJ, Hynes E, Lane WA. Verification of 2-D MEMS model using optical profiling techniques. *Opt Lasers Eng* 2001;36:169–83.
- [11] Tendela LP, Federico A, Kaufmann GH. Evaluation of the piezoelectric behavior produced by a thick-film transducer using digital speckle pattern interferometry. *Opt Lasers Eng* 2011;49:281–4.
- [12] Tendela LP, Galizzi GE, Federico A, Kaufmann GH. Measurement of nanometric displacements by correlating two speckle interferograms. *Appl Opt* 2011;50:1758–64.
- [13] Tendela LP, Galizzi GE, Federico A, Kaufmann GH. A fast method for measuring nanometric displacements by correlating speckle interferograms. *Opt Lasers Eng* 2012;50:170–5.
- [14] Xu W, Chang C, Hung YS, Kwan SK, Fung PCW. Order statistics correlation coefficient as a novel association measurement with applications to biosignal analysis. *IEEE Trans Signal Process* 2007;55:5552–63.
- [15] Davila A, Kaufmann GH, Kerr D. Digital processing of ESPI addition fringes. In: Jüptner W, Osten W, editors. *Fringe 93*. Berlin: Akademie Verlag; 1993. p. 339–46.
- [16] Rastogi PK. Measurement of static surface displacements, derivatives of displacements and three dimensional surface shape. In: Rastogi PK, editor. *Digital speckle pattern interferometry and related techniques*. Chichester, New York: Wiley; 2001. p. 142–224.